

## Article

# Preparation and Mechanical Properties of Layered Cu/Gr Composite Film

Qifeng Li <sup>1</sup>, Zhenbo Qin <sup>1,\*</sup>, Jingyun Chen <sup>1</sup>, Da-Hai Xia <sup>1</sup> , Yida Deng <sup>1</sup> , Yiwen Zhang <sup>1</sup>, Zhong Wu <sup>1,\*</sup> and Wenbin Hu <sup>1,2</sup>

<sup>1</sup> Tianjin Key Laboratory of Composite and Functional Materials, School of Material Science and Engineering, Tianjin University, Tianjin 300072, China; qifengli@tju.edu.cn (Q.L.); Jingyun19961229@163.com (J.C.); dahaixia@tju.edu.cn (D.-H.X.); yida.deng@tju.edu.cn (Y.D.); ywzsci@tju.edu.cn (Y.Z.); wbhu@tju.edu.cn (W.H.)

<sup>2</sup> Key Laboratory of Advanced Ceramics and Machining Technology (Ministry of Education), Tianjin University, Tianjin 300072, China

\* Correspondence: qinzhb@126.com (Z.Q.); zhong.wu@tju.edu.cn (Z.W.)

**Abstract:** Graphene (Gr) has proved its significant role as a reinforcement material in improving the strength of metal matrix composites due to its excellent mechanical properties. In this paper, Gr/Cu composite film with a layered structure was prepared by layering electrodeposition. The directional distribution of Gr in the Cu film was insured by this method, which gives play to its ultra-high-strength in a two-dimensional plane. In the meantime, the effect of electrodeposition time on the distribution structure of the Gr layer was studied. The structure analysis and mechanical properties test show that the strength of the layered Gr/Cu composite film is greatly improved compared to the pure Cu film. Furthermore, the strength of the composite film increases at the beginning and then decreases with the electrodeposition time of the Gr layer increasing, while the coverage and the degree for the layer stacking of Gr gradually increase in this process. In conclusion, the influence of different Gr distributions on the mechanical properties of the composite film has been studied by combining the experimental results with molecular dynamics simulation, which lays an effective foundation for further optimizing the structure of Gr in the layered composite film and improving the mechanical properties.

**Keywords:** Cu/Gr composite films; mechanical properties; molecular dynamics simulation



**Citation:** Li, Q.; Qin, Z.; Chen, J.; Xia, D.-H.; Deng, Y.; Zhang, Y.; Wu, Z.; Hu, W. Preparation and Mechanical Properties of Layered Cu/Gr Composite Film. *Coatings* **2021**, *11*, 502. <https://doi.org/10.3390/coatings11050502>

Academic Editor: Maria Cristina Tanzi

Received: 14 March 2021

Accepted: 21 April 2021

Published: 24 April 2021

**Publisher's Note:** MDPI stays neutral with regard to jurisdictional claims in published maps and institutional affiliations.



**Copyright:** © 2021 by the authors. Licensee MDPI, Basel, Switzerland. This article is an open access article distributed under the terms and conditions of the Creative Commons Attribution (CC BY) license (<https://creativecommons.org/licenses/by/4.0/>).

## 1. Introduction

Graphene (Gr), as an sp<sup>2</sup> hybridized two-dimensional material discovered in recent years [1], has attracted extensive attention due to its excellent thermal, electrical, and mechanical properties. The Young's modulus of monolayer graphene is 1 TPa and its tensile strength is 130 GPa [2], with an ultra-high specific surface area ( $\approx 2600 \text{ m}^2 \text{ g}^{-1}$ ) and ultra-low density ( $2.2 \text{ g cm}^{-3}$ ) [3]. Compared to carbon nanotubes and alumina particles, Gr is more suitable as a reinforcement for composite materials [4]. Cu matrix composites have been widely studied in view of their outstanding mechanical and physical properties, such as high tensile strength, high Young's modulus, superb wear resistance, splendid electric conductivity, and thermal conductivity [5–7]. As a potential high-performance material, Cu-based composite materials can be used for electronic packaging, electrical contact coatings, printed circuit board coatings, and fuel cell electrodes [8–10]. Therefore, researchers were committed to studying high-strength Cu/Gr composite materials.

Electrochemical co-deposition and powder metallurgy were the major methods for preparing Cu/Gr composite film. Researchers were devoted to the uniform dispersion of Gr in the Cu matrix and the improvement of interface strength. Song et al. [11] studied the effect of the concentration of Gr in a solution on the strength of the composite by the electrochemical co-deposition process. When the concentration was 0.5 g/L, the strength

of the composite was the highest, up to 360 MPa. Hwang et al. [3] prepared Gr/Cu composites with high interfacial strength through a molecular-level mixing process, and Jang et al. [12] prepared Gr/Cu composites with a strength of up to 841 MPa through chemical synthesis and hot-press sintering processes. As an anisotropic two-dimensional material, the directional distribution of Gr along the plane tensile direction can play its reinforcing effect more effectively, which is difficult to achieve by electrochemical co-deposition and powder metallurgy. The directional distribution of graphene can be achieved by the interlayer confinement of Cu with a multilayer structure. Kim et al. [13] prepared Gr/Cu and Gr/Ni layered composites by magnetron sputtering and chemical vapor deposition, respectively. The strength of the composites was increased by 2.5 times and 3.3 times, up to 1.5 GPa and 4.0 GPa, compared with Cu and Ni with only 0.5 vol% and 0.34 vol% of Gr added, respectively. The result confirmed the ultra-high enhancement effect of Gr when distributed along the plane. However, this preparation process is more complex and difficult to apply. The electrodeposition process is a simple and applicable method that can be used to prepare Cu with a multilayer structure. Cu with a multilayer structure also has broad application prospects in the field of Cu-based magnetic sensors. Deposition of Fe/Ni or Fe/Ni/Co layers on Cu wires is an effective way to fabricate magnetic sensors, but usually causes high stress [14,15], which can be solved by the electrodeposition of a Cu layer. Here, the multilayer Gr/Cu composite film may have greater advantages. The combined structure of multilayer Cu and magnetic layers also has important applications in magnetic materials, Vas'kovskiy et al. [16] and Amir et al. [17] have carried out meaningful research in this field. Therefore, the research of multilayer Cu and Gr/Cu composite film is of great significance.

Here, we proposed a simple and convenient layer-by-layer electrodeposition process that can prepare high-strength Gr/Cu composite film with a layered structure to achieve the directional distribution of Gr. By changing the electrodeposition time of the Gr layer, the structure distribution of Gr and the change of the mechanical properties of composite materials were studied, and the mechanism of the influence of Gr distribution on the mechanical properties was deeply explored in combination with molecular dynamics simulation.

## 2. Materials and Methods

### 2.1. Experimental Materials and Preparation Methods

All experimental reagents were analytical grade, and electrolytes were prepared with deionized water. The Cu layer and the Gr layer were prepared by different electrolyte systems and deposition methods. The Cu layer was deposited by the DC electrodeposition method with an electrolyte of  $\text{CuSO}_4 \cdot 5\text{H}_2\text{O}$  (200 g/L),  $\text{H}_2\text{SO}_4$  (60 g/L), and a current density of 5 A/dm<sup>2</sup>. A piece of copper was used as the anode plate, and the cathode plate was stainless steel with insulating tape on the back to avoid Cu deposition. The electrochemical reduction deposition of Gr adopted a three-electrode system, which consisted of a graphite plate (counter electrode), a saturated calomel electrode (reference electrode), and a stainless steel plate with a Cu layer as the working electrode. An aqueous solution containing sheet-shaped graphene oxide (GO, 0.5 g/L) was used as an electrolyte. The sheet-shaped GO used in this work was purchased from Nanjing Xianfeng Nanotechnology Co., Ltd., Nanjing, China, with a sheet diameter of 0.5–5  $\mu\text{m}$  and a thickness of 0.8–1.2 nm. The sheet-shaped structure of GO is favorable for the preparation of two-dimensional oriented distributed Gr. The deposition potential was pulsed, and each cycle was divided into positive potential (0.5 V, 2 s) and negative potential (−1.2 V, 3 s). The actual deposition time of Gr was the application time of negative potential. The deposition process was carried out in a constant temperature water bath (20–25 °C). The Cu layer and Gr layer were alternately deposited to ensure that the total deposition time of the Cu layer was 60 min (7.5 min  $\times$  8) and the number of Gr layers was 7. The microstructure evolution of graphene and the mechanical properties of the composite materials were studied by changing the electrodeposition time of the graphene layer.

## 2.2. Structural Characterization

The characterization of graphene in the composite materials used a composite material sample with a double-layer structure (Cu-Gr). An atomic force microscope (AFM, afm5500, Agilent, Palo Alto, CA, USA) was used to test the thickness and film diameter of the GO. The morphology of the Gr on the surface of the Cu layer was characterized by scanning electron microscope (SEM, JSM-7800F, JEOL, Shishima, Tokyo, Japan) and transmission electron microscope (TEM, JEM-2100 F, JEOL, Shishima, Tokyo, Japan), and the elemental composition of the sample was analyzed by an energy dispersive X-ray spectrometer (EDS, AMETEXK EDAX, JEOL, Shishima, Tokyo, Japan). The structure of the Gr was characterized by Fourier transform infrared spectrometer (FTIR, Nicolet Is10, Thermo Fisher, Waltham, MA, USA), X-ray photoelectron spectrometer (XPS, Axis Supra, Kratos, Trafford Park, Manchester, UK), and Raman spectrometer (Raman, LabRam ARAMIS, HORIBA, Kisshoin, Kyoto, Japan). The carbon content in the composite material was measured with an infrared carbon and sulfur analyzer (LECO CS844, St. Joseph, MI, USA).

## 2.3. Mechanical Performance Test

The tensile performance of the composite film was tested by using an Instron 5848 micro-mechanical with a tensile rate of 0.5 mm/min. The width of the samples was 3.2 mm and the thickness was the thickness of the sample itself (60–65  $\mu\text{m}$ ).

## 2.4. Molecular Dynamics Simulation

Figure 1 shows the pure Cu and Gr/Cu composite models with the size of  $20.5 \times 13.5 \times 4.0 \text{ nm}^3$ . The red atoms represent Cu, and the blue atoms represent Gr. The lattice orientations of the Cu matrix along X, Y, and Z are [100], [010], and [001] [18], respectively, and the configuration of Gr along the tensile direction was armchair. One end of the model was fixed along the X-axis direction, and the other end was stretched. The thickness of the constraint layer at both ends was 5 Å. Different models with different coverage and arrangement of graphene were named Gr/Cu-1, Gr/Cu-2, and Gr/Cu-3, respectively.

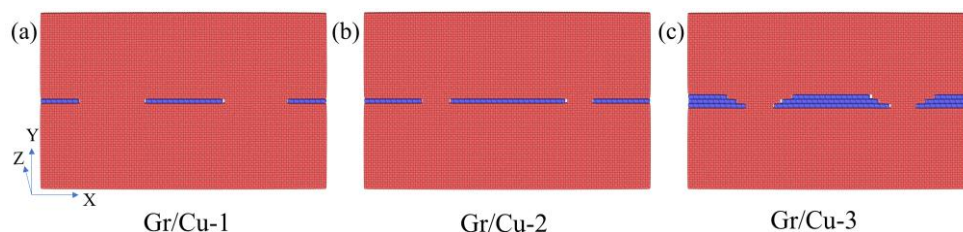


**Figure 1.** Two-dimensional view of (a) Gr/Cu-1, (b) Gr/Cu-2, and (c) Gr/Cu-3.

The tensile process of composites was simulated by molecular dynamics simulation. The atomic embedding method (EAM) interatomic potential was used to describe the interactions between Cu atoms [19]. The interactions between carbon atoms of Gr were described by the adaptive intermolecular reactive empirical bond order (AIREBO) potential [20]. The interaction between Cu and C was described by Lennard–Jones potential function, with a potential depth of 0.019996 eV and a size parameter of 3.225 Å [21]. All simulations apply periodic boundary conditions along the Z-axis. The nanocomposite models were equilibrated at the NPT ensemble at 300 K using the Nose–Hoover thermostat for 100 ps to reach an equilibrium state. During the stretching simulation, one end was fixed, and the other end was slowly stretched at a constant speed of 0.2 Å/ps in the X-axis direction. The MD simulations were carried out using the large-scale atomic molecular dynamics code LAMMPS [22]. Stress was calculated according to the Virial theorem. Ovito was used to visualize the deformation and fracture process.

### 3. Results and Discussion

#### 3.1. Characterizations of Structures and Morphologies

##### 3.1.1. Characterization of GO

The result of AFM measurement is shown in Figure 2a, indicating that GO has a thickness of about 0.8 nm. The thickness is in good consistency with the typical thickness of the observed single-layer GO (0.8 nm) [23,24]. Owing to the presence of epoxy and hydroxyl groups on both sides of the oxide surface, the typical thickness of single-layer GO shows a  $\sim 0.44$  nm increase in single-layer Gr thickness ( $\sim 0.36$  nm) [24,25]. The statistical results of multiple AFM measurements show that the thickness of graphene oxide is between 0.8–1.0 nm. The TEM image (Figure 2c) shows that the GO exhibited a kind of layered structure with curled edges. Figure 2d shows the FTIR spectrum of GO with four characteristic peaks at  $1042\text{ cm}^{-1}$ ,  $1616\text{ cm}^{-1}$ ,  $1714\text{ cm}^{-1}$ , and  $3155\text{ cm}^{-1}$ , corresponding to C–O, C=C, C=O, and –OH, respectively [26].

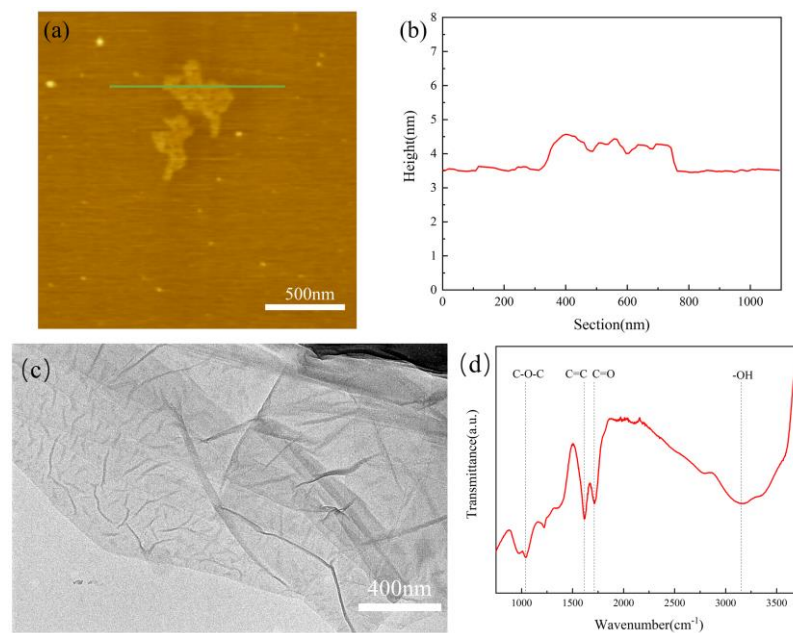


**Figure 2.** Microstructural characterizations of GO. (a) AFM image and (b) its height profile, (c) TEM image, and (d) FTIR spectrum.

##### 3.1.2. SEM Images and EDS of GO, Cu, and Cu-Gr

Figure 3 shows the SEM images and corresponding EDS of GO, Cu, and Cu-Gr. Gr with a folder structure can be seen in Cu-Gr, while not observed in Cu. Figure 3e,f shows the energy spectra of Cu and Cu-Gr, both of which have Cu, C, and O elements, but the peak intensity of carbon in Cu-Gr is significantly higher than that of pure Cu. As shown in Table 1, the carbon atom percentage in Cu-Gr is much higher than that of Cu. EDS mapping (Figure 4) of Cu and Cu-Gr shows that the Cu, C, and O elements were distributed uniformly in the film, but the presence of graphene in Cu-Gr makes it have a higher content and distribution density of C and O elements. The results indicate that Gr flakes were deposited onto the surface of the Cu layer.

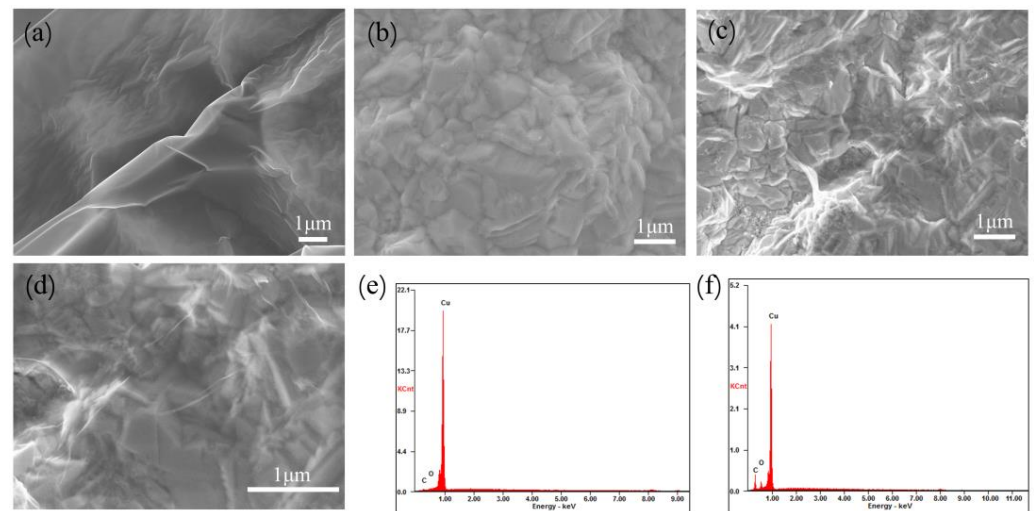


**Figure 3.** SEM images and EDS of the samples. (a) GO, (b) pure Cu, (c) low magnification and (d) high magnification of the Cu-Gr, EDS of the (e) Cu and (f) Cu-Gr.

**Table 1.** Proportion(at%) of EDS elements.

| Name  | Cu    | C     | O    |
|-------|-------|-------|------|
| Cu    | 88.40 | 7.95  | 3.65 |
| Gr/Cu | 54.83 | 37.45 | 7.71 |

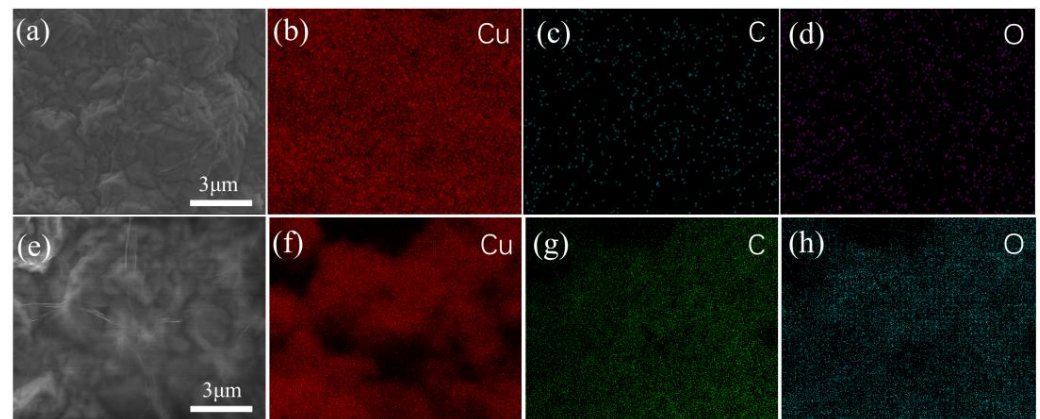


**Figure 4.** EDS elemental mapping analysis of the Cu and the Gr/Cu. SEM images of the (a) Cu and (e) Gr/Cu, and (b,f) the Cu element, (c,g) C element, and (d,h) O element.

### 3.1.3. TEM Images of Gr

TEM images of Gr with different deposition times are shown in Figure 5, indicating that the deposition of Gr mainly includes two processes: one is the increasing process of the Gr covered area; the other is the thickening process of the Gr stack. The stacking and agglomeration are due to the large specific surface area of graphene. Besides, during the deposition of Gr, the area where the Gr already exists on the Cu substrate has better conductivity, so that subsequent Gr is easily deposited on the original Gr to form a multilayer stack structure. The high magnification picture clearly shows the structure of a few-layer (Figure 5f) and multi-layer (Figure 5g) Gr.

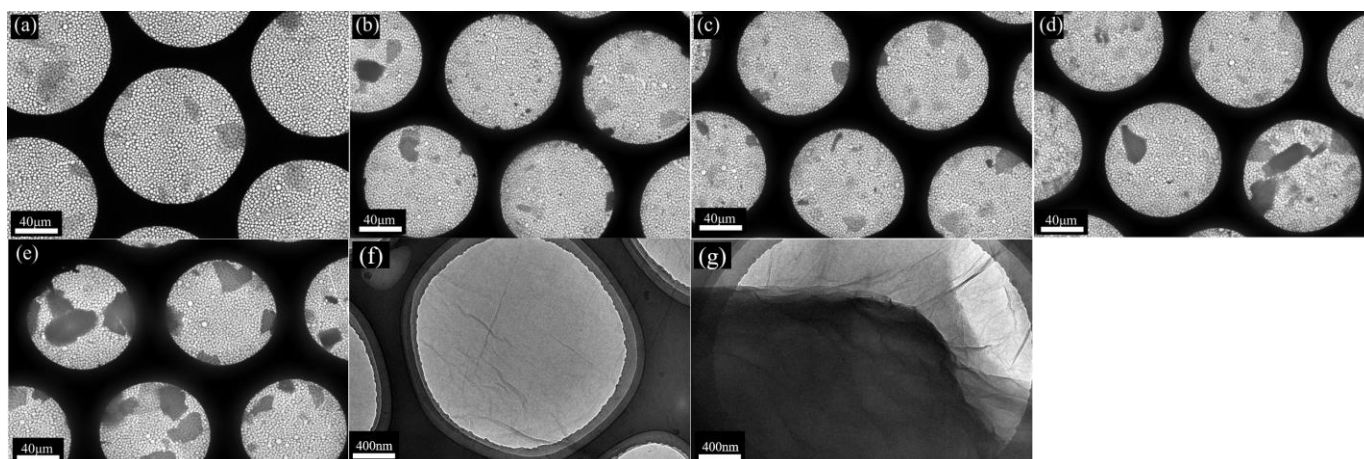


**Figure 5.** TEM images of the Gr (a) 120 s, (b) 180 s, (c) 240 s, (d) 300 s, and (e) 360 s. High magnification of the RGO with (f) fewer and (g) multiple layers.

### 3.1.4. XPS Spectra of GO and Cu-Gr

XPS test can characterize the types of carbon–oxygen bonds in GO and Cu-Gr with different deposition times and the changes of oxygen-containing functional groups before and after reduction. The XPS C1s spectra of GO and Cu-Gr based on Gaussian fitting are shown in Figure 6, and four peaks at 284.9 eV, 286.5 eV, 287.1 eV, and 288.9 eV are observed, representing C=C/C–C, C–O, C=O, and O=C–OH functional groups, respectively [27]. To reflect the reduction degree of oxygen-containing functional groups, we calculated the area ratio of each carbon–oxygen peak to carbon–carbon peak in GO and Gr, and the decreasing ratio of each bond type ratio in Cu-Gr to GO. The results are shown in Tables 2 and 3, respectively. The content of three kinds of oxygen-containing functional groups decreased significantly while the decreasing ratio of C–O is the largest, which fully indicates that GO removes a large amount of oxygen-containing functional groups to become Gr and deposits. Besides, this incomplete reduction allows the remaining oxygen-containing functional groups on the surface of the Gr to form a C–O–Cu bond with the Cu matrix, which is beneficial to the load transfer between Cu and Gr [3,4].

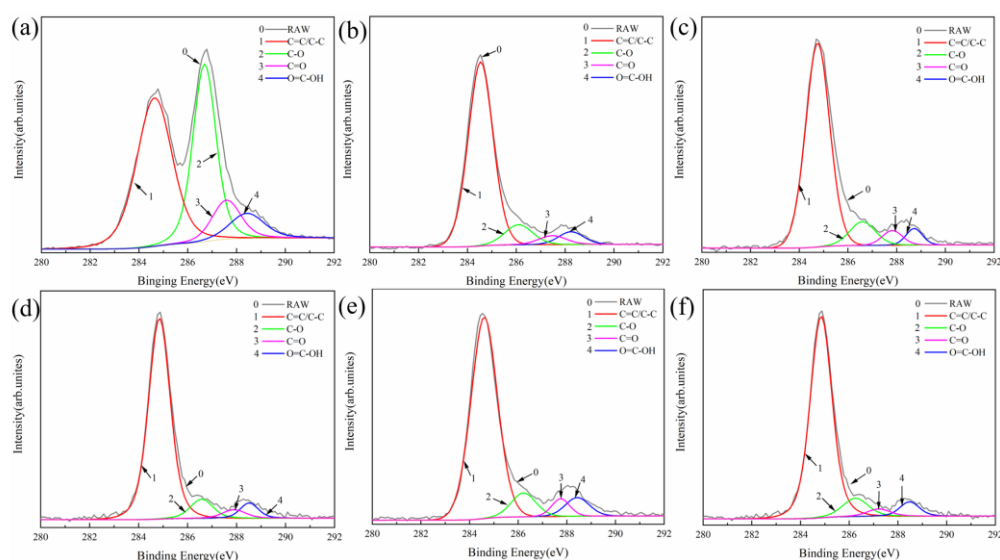


**Figure 6.** XPS C1s spectra of the (a) GO and Cu-Gr at (b) 120 s, (c) 180 s, (d) 240 s, (e) 300 s, and (f) 360 s.

**Table 2.** The peak area (A) ratios of the oxygen-containing functional bonds to the C-C bonds of the GO and Cu-Gr samples with different deposition times.

| Sample    | $A_{C-O}/A_{CC}$ | $A_{C=O}/A_{CC}$ | $A_{O-C-OH}/A_{CC}$ |
|-----------|------------------|------------------|---------------------|
| GO        | 0.823            | 0.206            | 0.159               |
| Gr/Cu-120 | 0.122            | 0.053            | 0.064               |
| Gr/Cu-180 | 0.124            | 0.059            | 0.054               |
| Gr/Cu-240 | 0.099            | 0.046            | 0.063               |
| Gr/Cu-300 | 0.110            | 0.059            | 0.079               |
| Gr/Cu-360 | 0.106            | 0.039            | 0.064               |

**Table 3.** The decreasing ratio of each bond type in Cu-Gr relative to GO (%).

| Sample    | C-O  | C=O  | O=C-OH |
|-----------|------|------|--------|
| Gr/Cu-120 | 85.2 | 74.3 | 59.7   |
| Gr/Cu-180 | 84.9 | 71.4 | 66.0   |
| Gr/Cu-240 | 87.9 | 77.6 | 60.4   |
| Gr/Cu-300 | 86.6 | 71.4 | 50.3   |
| Gr/Cu-360 | 87.1 | 81.1 | 59.7   |

### 3.1.5. Raman Spectra of GO and Cu-Gr

A Raman spectrometer was used to determine the structure of GO and Cu-Gr, the Raman spectrum (Figure 7) shows that the two main peaks of GO appear at  $1350\text{ cm}^{-1}$  and  $1600\text{ cm}^{-1}$ , which are called D peak and G peak, respectively [28]. The D peak reveals the defect density due to the lattice vibration leaving the Brillouin zone center, and the G peak was caused by  $sp^2$  hybridization of carbon atoms of in-plane vibration [29], the ratio of D peak to G peak ( $I_D/I_G$ ) can be used to characterize the defect degree of carbon materials [30]. Compared with GO, the position of the D peak and G peak of Cu-Gr shifted to between  $1328\text{--}1345\text{ cm}^{-1}$  and  $1580\text{--}1590\text{ cm}^{-1}$  (As shown in Table 4), respectively, which is called blue shift. The blue shift indicates the recovery of the hexagonal structure of carbon atoms in Gr [31]. Additionally, after the electrochemical reduction, the ratio of D peak to G peak of Gr-Cu is higher than that of GO (Table 4). This is due to the reduction of oxygen-containing functional groups on the surface of GO. After the reduction, some new defects were exposed [9]. Additionally, when the deposition time increases, the ratio of the D peak to the G peak of Cu-Gr increases gradually. This phenomenon can be explained by the deposition process of Gr. The deposition process of flake Gr is not completely uniform; as the electrodeposition time increases, the coverage of Gr on the Cu layer surface gradually increases. Therefore, a part of Gr tends to deposit on the surface of existing Gr to form new defect sites. The increase of deposition time will cause Gr to stack, leading to an increase of defects, and ultimately lead to an increase in the ratio of D peak to G peak.

## 3.2. Mechanical Properties Test

### 3.2.1. Mechanical Properties of Gr/Cu Composite Film

Figure 8 shows the stress–strain curve of Cu and Gr/Cu composite film. The Gr/Cu composite film has higher strength than pure Cu. As the electrodeposition time of the Gr layer increases, the strength of the composite materials increases gradually and then decreases, which reaches the maximum when the electrodeposition time is 240 s. The exact values are given in Table 5. In the initial stage of electrodeposition, the content of Gr in the composite film increases with the increase of electrodeposition time, and the enhancement effect is significant. After the electrodeposition time exceeds 240 s, the graphene in the composite film forms a multi-layer stacked structure with many defects, which reduces the bonding strength of the interface. Additionally, the decrease in the load-bearing capacity of graphene leads to a decrease in the strength of the composite film in turn.

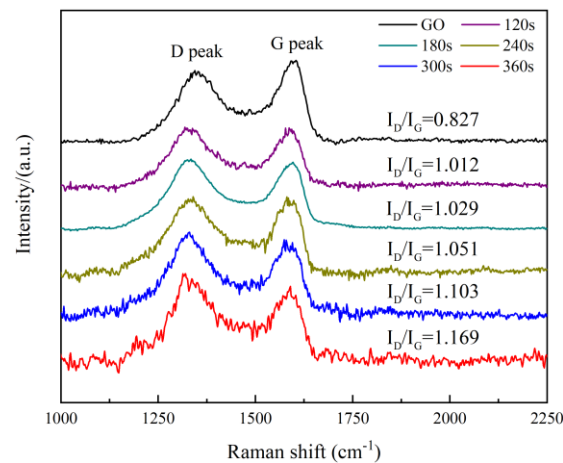


Figure 7. Raman spectra of the GO and Cu-Gr.

Table 4. The position and the ratio of D peak and G peak.

| Sample    | D Peak (cm <sup>-1</sup> ) | G Peak (cm <sup>-1</sup> ) | I <sub>D</sub> /I <sub>G</sub> |
|-----------|----------------------------|----------------------------|--------------------------------|
| GO        | 1350                       | 1600                       | 0.827                          |
| Gr/Cu-120 | 1335                       | 1590                       | 1.034                          |
| Gr/Cu-180 | 1331                       | 1593                       | 1.084                          |
| Gr/Cu-240 | 1334                       | 1588                       | 1.102                          |
| Gr/Cu-300 | 1329                       | 1585                       | 1.121                          |
| Gr/Cu-360 | 1341                       | 1589                       | 1.178                          |

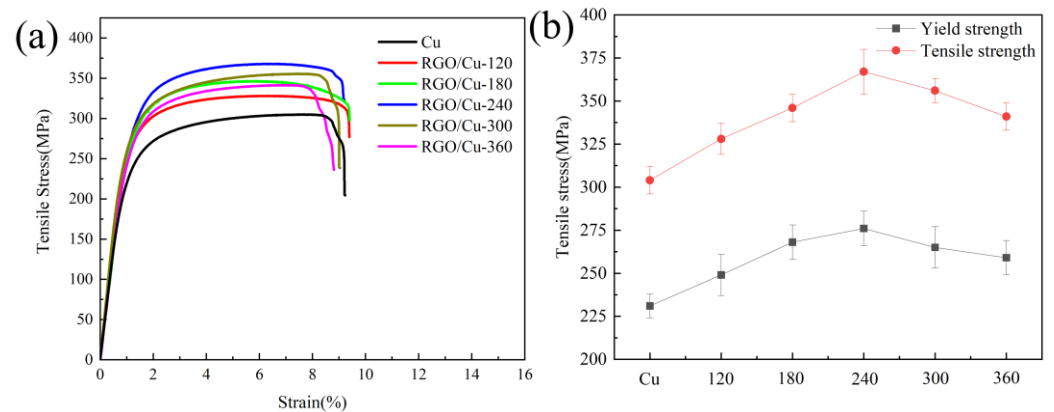


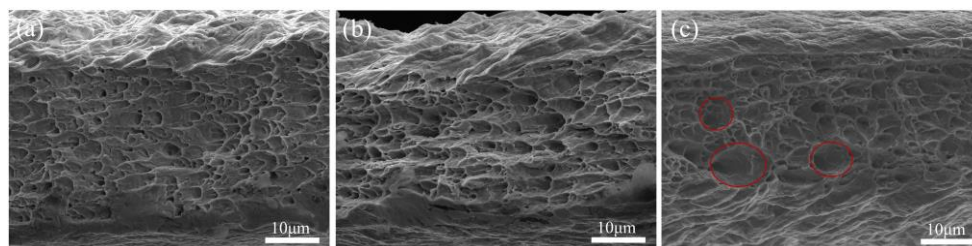
Figure 8. (a) Tensile stress–strain curves of Cu and Gr/Cu composite film with different deposition times of Gr, and (b) yield strength and tensile strength of Cu and Gr/Cu composite film with different deposition times of the Gr layer.

Table 5. Yield strength, tensile strength, and elongation of Cu and Gr/Cu composite film with different electrodeposition times.

| Sample    | Yield Strength/(MPa) | Tensile Strength / (MPa) | Elongation/(%) |
|-----------|----------------------|--------------------------|----------------|
| Cu        | 231                  | 304                      | 9.2            |
| Gr/Cu-120 | 249                  | 328                      | 9.4            |
| Gr/Cu-180 | 268                  | 346                      | 9.4            |
| Gr/Cu-240 | 276                  | 367                      | 9.2            |
| Gr/Cu-300 | 265                  | 356                      | 9.0            |
| Gr/Cu-360 | 259                  | 341                      | 8.8            |

### 3.2.2. Fracture Morphology of Gr/Cu Composite Film

Figure 9 shows the tensile fracture morphology of the Gr/Cu composite film. Many well-developed dimples can be seen in the figure, which means they are all plastic fractures. Figure 9a,b shows that Gr/Cu-120 and Gr/Cu-240 have similar fracture morphologies and uniformly distributed dimples, indicating that both have good elongation (9.4% and 9.2%, Table 5). Figure 9c shows that there are some larger dimples (Circled area) in the fracture morphology of Gr/Cu-360. The reason for this phenomenon is that the stacking of Gr (Figure 5e,g) leads to poor adhesion of the Gr/Cu interface, which will develop into voids during stretching. This process also resulted in a decrease in elongation (8.8%, Table 5).



**Figure 9.** Fracture surfaces of the Gr/Cu composite film at (a) 120 s, (b) 240 s, and (c) 360 s.

### 3.3. Molecular Dynamics (MD) Simulations

Molecular dynamics simulations were used to verify the influence mechanism of Gr layers and stacking on the mechanical properties of composite materials. In previous molecular dynamics simulation studies, the strength of Gr/Cu composites was generally higher than that of Cu [19,21,32]. Guo et al. [32] used molecular dynamics simulation at 300 K to get the tensile strength of copper to be 8.1 GPa, and the strength of Cr/Cu composite material was 9.5 GPa. Figure 10 shows the tensile simulated stress–strain curve of the Gr/Cu composite film, the illustration is an enlarged view of the marked area. The strengths of Gr/Cu-1, Gr/Cu-2, and Gr/Cu-3 are 9.65 GPa, 10.28 GPa, and 9.0 GPa, respectively, which are higher than that of copper under the same conditions (8.1 GPa). The strength obtained by the tensile simulation shows a trend of increasing first and then decreasing, which is the same as the result obtained in the experiment.

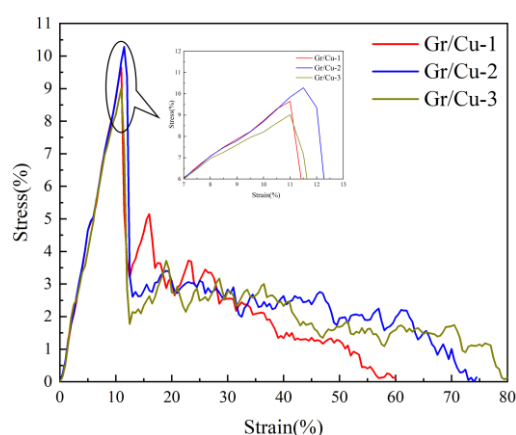


**Figure 10.** Tensile simulation stress–strain curves of Gr/Cu composites.

Figures 11–13 show the atomic configuration changes of the three models under different tensile strains ( $\epsilon$ ). Gr/Cu-1 and Gr/Cu-2 have similar deformation and fracture processes, which are combined by the following two factors: one is the plastic deformation of the copper matrix, and the other is the initiation and expansion of Gr/Cu interface defects. During the stretching process, the composite materials reach their maximum strength and begin to undergo plastic deformation, the Cu matrix slides along the Gr.

At the same time, a cavity starts to grow at the interface, which further expands under the action of stretching, leading to the fracture failure process of the composite materials. Besides, the size of Gr in Gr/Cu-2 is larger than that of Gr/Cu-1, which has a better hindering effect on the deformation of the Cu matrix. The deformation and fracture process of Gr/Cu-3 is illustrated in Figure 13. Multilayer Gr forms larger voids (Figure 13a,b) in the Cu matrix, which reduces the load-bearing effect of Gr and leads to a decrease in strength. As the strain continues to increase (Figure 13c), delamination occurs between multilayer Gr. As the strain increases (Figure 13d), obvious interlayer sliding is formed, and a larger void also appears at the Gr/Cu interface.

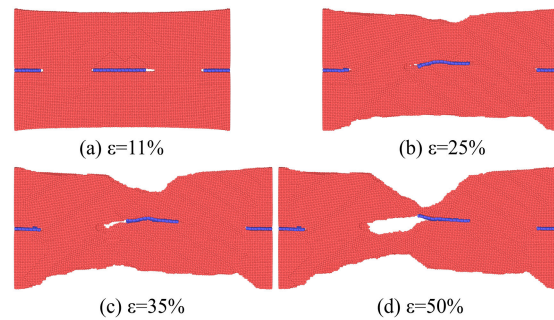


**Figure 11.** Atomic configuration diagram of Gr/Cu-1 under different strains during stretching. (a)  $\varepsilon = 11\%$ , (b)  $\varepsilon = 25\%$ , (c)  $\varepsilon = 35\%$  and (d)  $\varepsilon = 50\%$ .

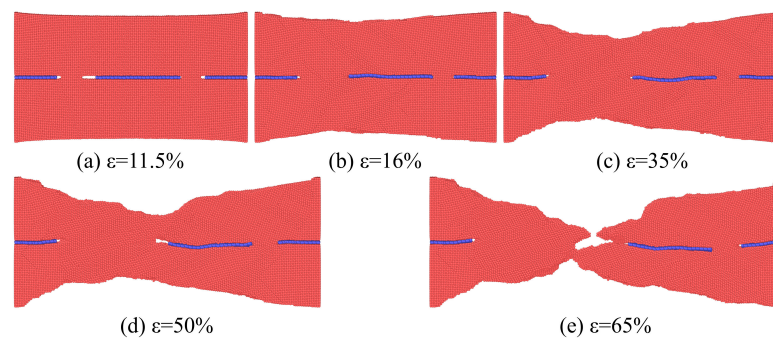


**Figure 12.** Atomic configuration diagram of Gr/Cu-2 under different strains during stretching. (a)  $\varepsilon = 11.5\%$ , (b)  $\varepsilon = 16\%$ , (c)  $\varepsilon = 35\%$ , (d)  $\varepsilon = 50\%$  and (e)  $\varepsilon = 65\%$ .

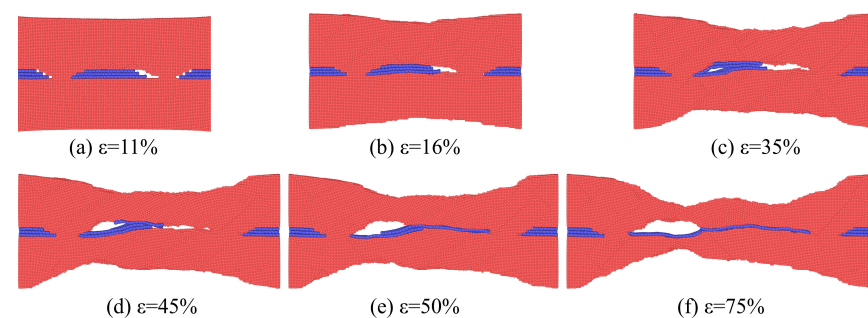


**Figure 13.** Atomic configuration diagram of Gr/Cu-3 under different strains during stretching. (a)  $\varepsilon = 11\%$ , (b)  $\varepsilon = 16\%$ , (c)  $\varepsilon = 35\%$ , (d)  $\varepsilon = 45\%$ , (e)  $\varepsilon = 50\%$  and (f)  $\varepsilon = 75\%$ .

The trend of dislocation density in Gr/Cu composites with increasing strain is shown in Figure 14. The dislocation density of Gr/Cu-2 is significantly higher than that of Gr/Cu-1 and Gr/Cu-3, which matches the strength change of the composite materials. Figures 15–20 show the crystal structure, dislocation distribution, and stress distribution diagrams of three composite materials under different strains. Gr/Cu-1 and Gr/Cu-2 have similar models.

Under tensile strain, the composite material undergoes a martensitic transformation, and part of the crystal structure changes from FCC to HCP, followed by dislocations that occur at the interface between Gr and Cu (Figures 15a and 17a). As a reinforcing phase, Gr provides an impermeable interface for the dislocations in the composite material to form dislocation plugging. This high dislocation density makes dislocation slip more difficult, hinders the plastic deformation of the Cu matrix, and improves the strength of the composite materials [33]. In Gr/Cu-2, the dislocation hindering effect is more obvious due to a higher dislocation density and strength caused by the higher content of Gr. The stress distribution state also confirms this statement (Figures 16a and 18a). The subsequent fracture of the two composite materials is mainly dominated by the pores between one end of the Gr and the matrix: Gr/Cu-1 has produced obvious cavities, dislocation plugging, and stress concentration when the tensile strain is 35%, while the strain point that produces obvious voids and stress concentration in Cu-2 is much higher than that of Gr/Cu-1.

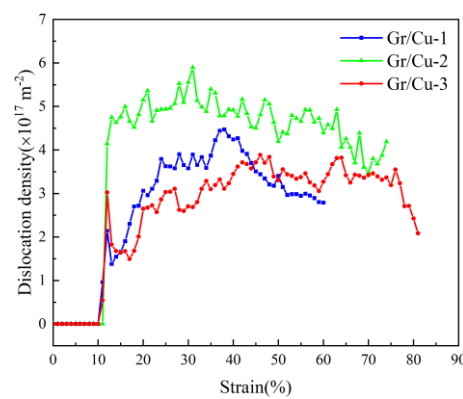


Figure 14. The dislocation density of Gr/Cu composites under different strains.

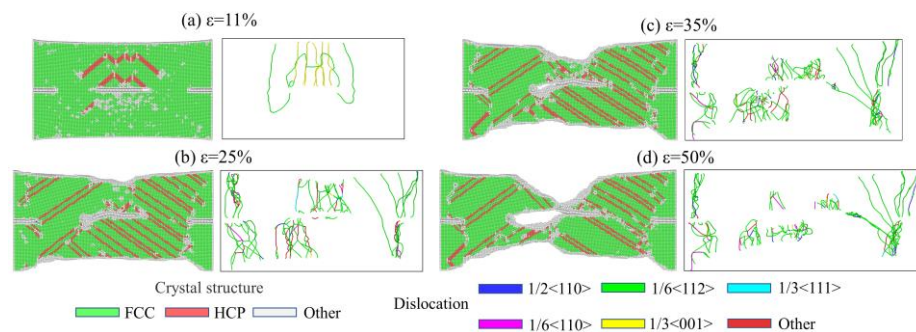


Figure 15. Crystal structure and dislocation line distribution of Gr/Cu-1 under different strains. (a)  $\epsilon = 11\%$ , (b)  $\epsilon = 25\%$ , (c)  $\epsilon = 35\%$  and (d)  $\epsilon = 50\%$ .

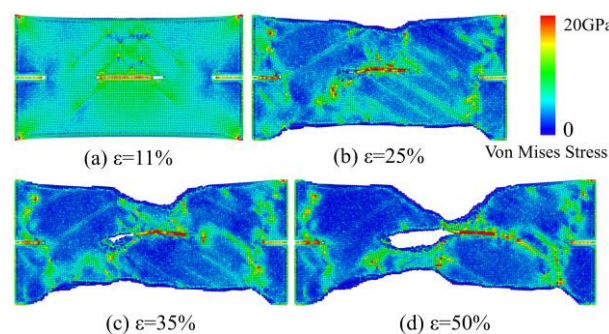
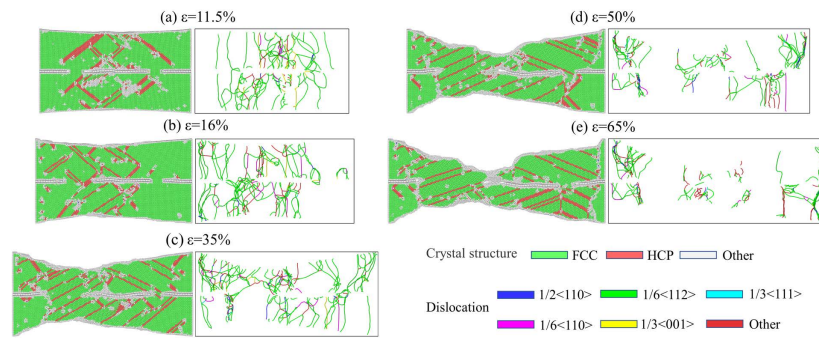
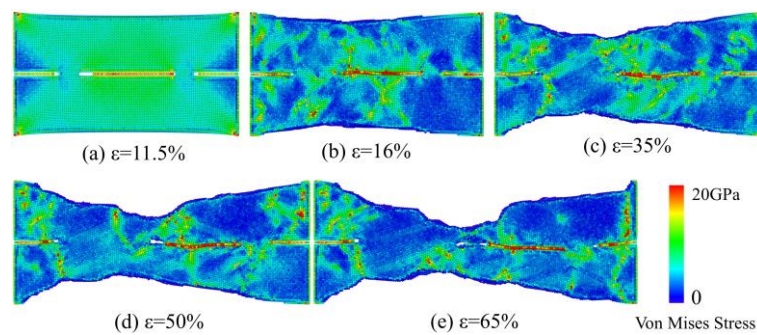


Figure 16. Stress distribution of Gr/Cu-1 under different strains. (a)  $\epsilon = 11\%$ , (b)  $\epsilon = 25\%$ , (c)  $\epsilon = 35\%$  and (d)  $\epsilon = 50\%$ .



**Figure 17.** Crystal structure and dislocation line distribution of Gr/Cu-2 under different strains. (a)  $\epsilon = 11.5\%$ , (b)  $\epsilon = 16\%$ , (c)  $\epsilon = 35\%$ , (d)  $\epsilon = 50\%$  and (e)  $\epsilon = 65\%$ .



**Figure 18.** Stress distribution of Gr/Cu-2 under different strains. (a)  $\epsilon = 11.5\%$ , (b)  $\epsilon = 16\%$ , (c)  $\epsilon = 35\%$ , (d)  $\epsilon = 50\%$  and (e)  $\epsilon = 65\%$ .

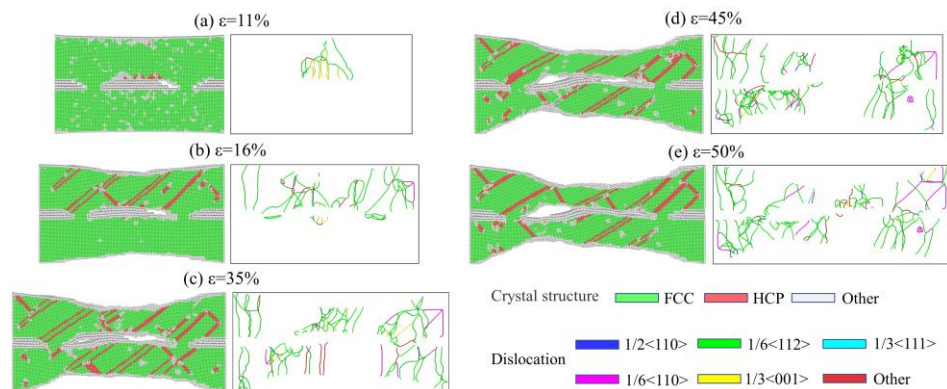


**Figure 19.** Crystal structure and dislocation line distribution of Gr/Cu-3 under different strains. (a)  $\epsilon = 11\%$ , (b)  $\epsilon = 16\%$ , (c)  $\epsilon = 35\%$ , (d)  $\epsilon = 45\%$  and (e)  $\epsilon = 50\%$ .

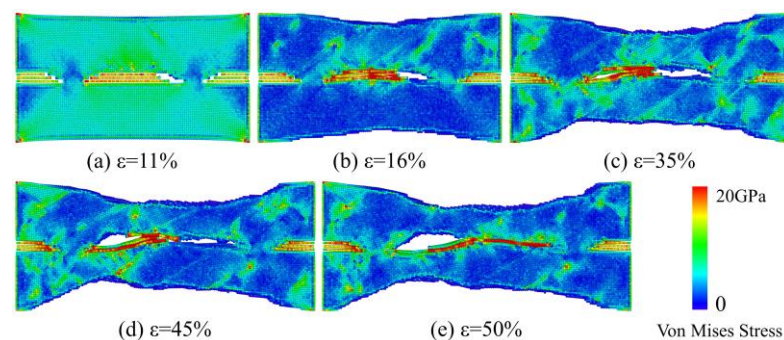


**Figure 20.** Stress distribution of Gr/Cu-3 under different strains. (a)  $\epsilon = 11\%$ , (b)  $\epsilon = 16\%$ , (c)  $\epsilon = 35\%$ , (d)  $\epsilon = 45\%$  and (e)  $\epsilon = 50\%$ .

For Gr/Cu-3 (Figures 19 and 20), the dislocation density and high-stress region in the matrix are lower than those of Gr/Cu-1 and Gr/Cu-2 when the strain is 11%, which is due to the weak interface between the end of the multilayer Gr and the Cu matrix [4,34]. Additionally, more obvious cavities are formed during the tensile process, which makes the dislocation move to the free surface of the cavity and annihilates, resulting in the decrease in the strength of the composite. As the strain continues to increase (Figure 19c,d and Figure 20c,d), the van der Waals force between the layers of stacked Gr is weak, which makes it easy to form interlaminar shear and delamination [35,36]. As a result, with the bonding and load transfer effects of the composite weakened [37], the dislocation density decreases and the stress of the middle layer of Gr is significantly less than that of the outer two layers (Figure 20c,d). As the strain continues to increase (Figures 19e and 20e), the multilayer Gr interface is seriously delaminated and the voids at the interface further increase, causing the Gr to be unable to effectively bear the load and a decrease in the mechanical properties of the composite material.

In summary, the increase in the coverage of Gr can effectively hinder the movement of dislocations in the matrix to increase the strength, while the stacking of multilayer irregular Gr will reduce the interface bonding strength between Gr and Cu in the composites, resulting in the generation of interface voids (which is also verified in the tensile fracture). At the same time, the interlayer shear and delamination of the multilayer Gr during the stretching process reduce the load transfer efficiency, and the combined effect of the two leads to the reduction in the strength of the composite material.

#### 4. Conclusions

In this paper, a layer-by-layer electrodeposition process was used to prepare layered Cu/Gr composite film. The tensile performance measurement shows that the tensile strength of the composite film was greatly improved compared to the pure Cu film. Combining structural analysis and molecular dynamics simulations, we studied the influence of electrodeposition time on the distribution structure of Gr between layers and the mechanical properties of composite materials: with the increase of Gr electrodeposition time, the coverage of Gr and the degree of layer stacking gradually increase, and the strength of the composite film shows a trend of increasing first and then decreasing. The influence mechanism is studied through TEM characterization and molecular dynamics simulation: when the electrodeposition time is short (120–240 s), the deposition process of Gr is mainly to increase the coverage. During this period, the increase of the Gr content can increase the interface area between the Gr and the Cu matrix, thereby increasing the blocking effect of Gr on dislocation movement and stress transfer efficiency, and then improve the strength of the composite film; when the electrodeposition time is too long, the deposition process of Gr is mainly the increase of the stacking degree. The stacked Gr forms a weak interface bond in the Cu matrix, resulting in the generation of interface voids, and the interlaminar shear and delamination of multilayer Gr in the stretching process reduce the load transfer process, which reduces the strength of the composite film.

**Author Contributions:** Conceptualization, Z.Q. and Z.W.; methodology, Q.L.; software, Q.L. and Z.W.; validation, W.H.; formal analysis, Z.Q.; investigation, Q.L. and J.C.; resources, D.-H.X. and Y.D.; data curation, Y.Z.; writing—original draft preparation, Q.L.; writing—review and editing, Z.W.; visualization, Q.L. and Y.Z.; supervision, Z.W.; project administration, W.H. and Y.D.; funding acquisition, Z.W. All authors have read and agreed to the published version of the manuscript.

**Funding:** This research was funded by the National Natural Science Foundation of China (No. 51971155, No. 52001226 and No. 52031007).

**Institutional Review Board Statement:** Not applicable.

**Informed Consent Statement:** Not applicable.

**Data Availability Statement:** The data presented in this study are available in this article.

**Conflicts of Interest:** The authors declare no conflict of interest.

## References

1. Meyer, J.C.; Geim, A.K.; Katsnelson, M.I.; Novoselov, K.S.; Booth, T.J.; Roth, S. The structure of suspended graphene sheets. *Nature* **2007**, *446*, 60–63. [[CrossRef](#)] [[PubMed](#)]
2. Varol, T.; Canakci, A. Microstructure, electrical conductivity and hardness of multilayer graphene/Copper nanocomposites synthesized by flake powder metallurgy. *Met. Mater. Int.* **2015**, *21*, 704–712. [[CrossRef](#)]
3. Hwang, J.; Yoon, T.; Jin, S.H.; Lee, J.; Kim, T.S.; Hong, S.H.; Jeon, S. Enhanced Mechanical Properties of Graphene/Copper Nanocomposites Using a Molecular-Level Mixing Process. *Adv. Mater.* **2013**, *25*, 6724–6729. [[CrossRef](#)] [[PubMed](#)]
4. Chen, F.Y.; Ying, J.M.; Wang, Y.F.; Du, S.Y.; Liu, Z.P.; Huang, Q. Effects of graphene content on the microstructure and properties of copper matrix composites. *Carbon* **2016**, *96*, 836–842. [[CrossRef](#)]
5. Liu, Q.; He, X.B.; Ren, S.B.; Zhang, C.; Liu, T.T.; Qu, X.H. Thermophysical properties and microstructure of graphite flake/copper composites processed by electroless copper coating. *J. Alloys Compd.* **2014**, *587*, 255–259. [[CrossRef](#)]
6. Tjong, S.C.; Ma, Z.Y. Microstructural and mechanical characteristics of in situ metal matrix composites. *Mater. Sci. Eng. R Rep.* **2000**, *29*, 49–113. [[CrossRef](#)]
7. Jiang, X.S.; Liu, W.X.; Li, J.R.; Shao, Z.Y.; Zhu, D.G. Microstructures and mechanical properties of Cu/Ti<sub>3</sub>SiC<sub>2</sub>/C/MWCNTs composites prepared by vacuum hot-pressing sintering. *J. Alloys Compd.* **2015**, *618*, 700–706.
8. Yoo, S.J.; Han, S.H.; Kim, W.J. A combination of ball milling and high-ratio differential speed rolling for synthesizing carbon nanotube/copper composites. *Carbon* **2013**, *61*, 487–500. [[CrossRef](#)]
9. Song, G.; Yang, Y.; Fu, Q.; Pan, C. Preparation of Cu-Graphene Composite Thin Foils via DC Electro-Deposition and Its Optimal Conditions for Highest Properties. *J. Electrochem. Soc.* **2017**, *164*, D652–D659. [[CrossRef](#)]
10. Xie, G.X.; Forslund, M.; Pan, J.S. Direct Electrochemical Synthesis of Reduced Graphene Oxide (rGO)/Copper Composite Films and Their Electrical/Electroactive Properties. *ACS Appl. Mater. Interfaces* **2014**, *6*, 7444–7455. [[CrossRef](#)]
11. Song, G.S.; Wang, Z.C.; Gong, Y.N.; Yang, Y.P.; Fu, Q.; Pan, C.X. Direct determination of graphene amount in electrochemical deposited Cu-based composite foil and its enhanced mechanical property. *RSC Adv.* **2017**, *7*, 1735–1742. [[CrossRef](#)]
12. Jang, H.; Yoo, S.; Quevedo, M.; Choi, H. Effect of processing route on mechanical and thermal properties of few-layered graphene (FLG)-reinforced copper matrix composites. *J. Alloys Compd.* **2018**, *754*, 7–13. [[CrossRef](#)]
13. Kim, Y.; Lee, J.; Yeom, M.S.; Shin, J.W.; Kim, H.; Cui, Y.; Kysar, J.W.; Hone, J.; Jung, Y.; Jeon, S.; et al. Strengthening effect of single-atomic-layer graphene in metal-graphene nanolayered composites. *Nat. Commun.* **2013**, *4*, 7. [[CrossRef](#)]
14. Favieres, C.; Aroca, C.; Sanchez, M.C.; Madurga, V. Matteucci effect as exhibited by cylindrical CoP amorphous multilayers. *J. Appl. Phys.* **2000**, *87*, 1889–1898. [[CrossRef](#)]
15. Kurlyandskaya, G.V.; Garcia-Miquel, H.; Vazquez, M.; Svalov, A.V.; Vas'kovskiy, V.O. Longitudinal magnetic bistability of electroplated wires. *J. Magn. Magn. Mater.* **2002**, *249*, 34–38. [[CrossRef](#)]
16. Vas'kovskii, V.O.; Svalov, A.V.; Yuvchenko, A.A.; Kataeva, E.A. Interlayer coupling and magnetization process in Co/X/Gd-Co (X = Si, Ti, Cu) artificial ferrimagnets. *Phys. Met. Metallogr.* **2006**, *101*, S84–S86. [[CrossRef](#)]
17. Amir, S.M.; Gupta, M.; Gupta, A. Surfactant controlled interfacial alloying in thermally evaporated Cu/Co multilayers. *J. Alloys Compd.* **2012**, *522*, 9–13. [[CrossRef](#)]
18. Gu, Y.T.; Zhan, H.F. MD investigations for mechanical properties of copper nanowires with and without surface defects. *Int. J. Comput. Methods* **2012**, *9*, 1240003. [[CrossRef](#)]
19. Duan, K.; Zhu, F.L.; Tang, K.; He, L.P.; Chen, Y.M.; Liu, S. Effects of chirality and number of graphene layers on the mechanical properties of graphene-embedded copper nanocomposites. *Comput. Mater. Sci.* **2016**, *117*, 294–299. [[CrossRef](#)]
20. Yang, Z.Y.; Wang, D.D.; Lu, Z.X.; Hu, W.J. Atomistic simulation on the plastic deformation and fracture of bio-inspired graphene/Ni nanocomposites. *Appl. Phys. Lett.* **2016**, *109*, 5. [[CrossRef](#)]
21. Hua, J.; Duan, Z.R.; Song, C.; Liu, Q.L. Molecular dynamics study on the tensile properties of graphene/Cu nanocomposite. *Int. J. Comput. Mat. Sci. Eng.* **2017**, *6*, 15. [[CrossRef](#)]
22. Plimpton, S. Fast Parallel Algorithms for Short-Range Molecular Dynamics. *J. Comput. Phys.* **1995**, *117*, 1–19. [[CrossRef](#)]
23. Akhavan, O. Photocatalytic reduction of graphene oxides hybridized by ZnO nanoparticles in ethanol. *Carbon* **2011**, *49*, 11–18. [[CrossRef](#)]
24. Schniepp, H.C.; Li, J.L.; McAllister, M.J.; Sai, H.; Herrera-Alonso, M.; Adamson, D.H.; Prud'homme, R.K.; Car, R.; Saville, D.A.; Aksay, I.A. Functionalized single graphene sheets derived from splitting graphite oxide. *J. Phys. Chem. B* **2006**, *110*, 8535–8539. [[CrossRef](#)] [[PubMed](#)]
25. McAllister, M.J.; Li, J.L.; Adamson, D.H.; Schniepp, H.C.; Abdala, A.A.; Liu, J.; Herrera-Alonso, M.; Milius, D.L.; Car, R.; Prud'homme, R.K.; et al. Single sheet functionalized graphene by oxidation and thermal expansion of graphite. *Chem. Mater.* **2007**, *19*, 4396–4404. [[CrossRef](#)]
26. Wang, Y.; Zhao, Y.; Bao, T.J.; Li, X.; Su, Y.Q.; Duan, Y.X. Preparation of Ni-reduced graphene oxide nanocomposites by Pd-activated electroless deposition and their magnetic properties. *Appl. Surf. Sci.* **2012**, *258*, 8603–8608. [[CrossRef](#)]
27. Dong, X.C.; Su, C.Y.; Zhang, W.J.; Zhao, J.W.; Ling, Q.D.; Huang, W.; Chen, P.; Li, L.J. Ultra-large single-layer graphene obtained from solution chemical reduction and its electrical properties. *Phys. Chem. Chem. Phys.* **2010**, *12*, 2164–2169. [[CrossRef](#)] [[PubMed](#)]
28. Malard, L.M.; Pimenta, M.A.; Dresselhaus, G.; Dresselhaus, M.S. Raman spectroscopy in graphene. *Phys. Rep.* **2009**, *473*, 51–87. [[CrossRef](#)]

29. Singh, B.P.; Nayak, S.; Nanda, K.K.; Jena, B.K.; Bhattacharjee, S.; Besra, L. The production of a corrosion resistant graphene reinforced composite coating on copper by electrophoretic deposition. *Carbon* **2013**, *61*, 47–56. [[CrossRef](#)]
30. Zong, M.; Huang, Y.; Wu, H.W.; Zhao, Y.; Liu, P.B.; Wang, L. Facile preparation of RGO/Cu<sub>2</sub>O/Cu composite and its excellent microwave absorption properties. *Mater. Lett.* **2013**, *109*, 112–115. [[CrossRef](#)]
31. Zhang, Y.W.; Chang, G.H.; Liu, S.; Tian, J.Q.; Wang, L.; Lu, W.B.; Qin, X.Y.; Sun, X.P. Microwave-assisted, environmentally friendly, one-pot preparation of Pd nanoparticles/graphene nanocomposites and their application in electrocatalytic oxidation of methanol. *Catal. Sci. Technol.* **2011**, *1*, 1636–1640. [[CrossRef](#)]
32. Guo, J.; Wang, B.; Yang, Z. Molecular dynamics simulations on the mechanical properties of graphene/Cu composites. *Acta Mater. Compos. Sin.* **2014**, *31*, 152–157.
33. Jiang, R.R.; Zhou, X.F.; Fang, Q.L.; Liu, Z.P. Copper-graphene bulk composites with homogeneous graphene dispersion and enhanced mechanical properties. *Mater. Sci. Eng. A* **2016**, *654*, 124–130. [[CrossRef](#)]
34. Yue, H.Y.; Yao, L.H.; Gao, X.; Zhang, S.L.; Guo, E.; Zhang, H.; Lin, X.Y.; Wang, B. Effect of ball-milling and graphene contents on the mechanical properties and fracture mechanisms of graphene nanosheets reinforced copper matrix composites. *J. Alloys Compd.* **2017**, *691*, 755–762. [[CrossRef](#)]
35. Ma, G.S.; Chen, Y.B.; Xia, L.; Zhan, Y.F.; Zhong, B.; Yang, H.; Huang, L.N.; Xiong, L.; Huang, X.X.; Wen, G.W. Mechanical and thermal properties of Graphene nanoplates (GNPs)/Lithium aluminosilicate (LAS) composites: An analysis based on mathematical model and experiments. *Ceram. Int.* **2020**, *46*, 10903–10909. [[CrossRef](#)]
36. Pratik, A.; Biswal, S.K.; Haridoss, P. Impact of enhanced interfacial strength on physical, mechanical and tribological properties of copper/reduced graphene oxide composites: Microstructural investigation. *Ceram. Int.* **2020**, *46*, 22539–22549. [[CrossRef](#)]
37. Chen, Y.K.; Zhang, X.; Liu, E.Z.; He, C.N.; Shi, C.S.; Li, J.J.; Nash, P.; Zhao, N.Q. Fabrication of in-situ grown graphene reinforced Cu matrix composites. *Sci. Rep.* **2016**, *6*, 9. [[CrossRef](#)]